Gapless quantum spin liquid ground state in the spin-1 antiferromagnet 6HB-$Ba_3NiSb_2O_9$

J. A. Quilliam,[1,2] F. Bert,[2] A. Manseau,[1] C. Darie,[3] C. Guillot-Deudon,[4] C. Payen,[4] C. Baines,[5] A. Amato,[5] and P. Mendels[2]

[1]*Institut Quantique and Département de Physique, Université de Sherbrooke, 2500 boul. de l'Université, Sherbrooke, Québec, Canada J1K 2R1*

[2]*Laboratoire de Physique des Solides, CNRS, Univ. Paris-Sud, Université Paris-Saclay, 91405 Orsay Cedex, France*

[3]*Institut Néel, CNRS and UJF, BP 166, 38042 Grenoble Cedex, France*

[4]*Institut des Matériaux Jean Rouxel, UMR 6502 Université de Nantes, CNRS, 2 rue de la Houssinière, BP 32229, 44322 Nantes Cedex 3, France*

[5]*Laboratory for Muon Spin Spectroscopy, Paul Scherrer Institute, CH-5232 Villigen PSI, Switzerland*

(Received 3 February 2016; published 27 June 2016)

We present an in-depth study of the magnetic properties of the spin-1 antiferromagnet 6HB-$Ba_3NiSb_2O_9$. μSR measurements demonstrate that this material shows no static magnetism down to temperatures as low as 20 mK, making it a likely candidate for a quantum spin liquid state. ^{121}Sb NMR shift measurements show that the local, intrinsic susceptibility levels off at temperatures below $\sim$60 K. The NMR spin-lattice relaxation rate $1/T_1$ is essentially constant in temperature and the muon relaxation rate exhibits a low-temperature relaxation plateau, all indications of gapless spin excitations. Our local probe measurements are discussed in the context of several theories proposed for this material.

DOI: 10.1103/PhysRevB.93.214432

I. INTRODUCTION

In the presence of strong magnetic frustration and quantum fluctuations, the usual long-range Néel order of an antiferromagnetic spin system can give way to a much more exotic ground state known as a quantum spin liquid (QSL) that exhibits long-range spin entanglement and supports fractional spin excitations (for example spinons) [1]. Many decades of theoretical interest have led to the relatively recent discovery of several likely QSL states in materials with spin-1/2 moments on kagome lattices [2,3] and triangular lattices near to a Mott transition [4,5]. As we begin to understand these materials, a logical next step is to consider a middle ground between quantum and classical limits by studying $S = 1$ systems on frustrated lattices. Just as in the case of one-dimensional spin chains [6], we may expect significant, qualitative differences between the $S = 1/2$ and $S = 1$ cases.

A particularly appealing $S = 1$ frustrated system is the triangular antiferromagnet 6HB-$Ba_3NiSb_2O_9$ [7]. Although the ambient pressure 6HA phase of $Ba_3NiSb_2O_9$ orders [8,9], the 6HB phase, synthesized at pressures $\gtrsim$2 GPa [10], has shown no indications of magnetic order in thermodynamic quantities, but instead a T-linear specific heat C and a constant magnetic susceptibility χ after subtraction of a small Curie tail [7] (see Fig. 1). The idea of a Fermi surface of spinons has been invoked [7] and a large Wilson ratio $W = 4\pi^2 k_B^2 \chi_0 / 3g^2\mu_B^2\gamma \simeq 5.6$ has been obtained, suggestive of strong spinon correlations. These findings have triggered a great deal of theoretical interest in triangular spin-1 models [11–16]. In this paper we investigate the magnetic properties of 6HB-$Ba_3NiSb_2O_9$ and, through an in-depth local-probe study, show that it does appear to exhibit a gapless QSL ground state.

Studies of the related material $Ba_3CuSb_2O_9$ have highlighted the likelihood and importance of structural disorder in such a structure. $Ba_3CuSb_2O_9$ is thought to have a triangular lattice of Sb^{5+}-Cu^{2+} "dumbbells," the orientations of which are quenched almost randomly during crystal growth [17]. The resulting magnetic Cu lattices have been argued to either exhibit correlated disorder with a local honeycomb structure [17] or short-range stripe order [18]. $Ba_3CuSb_2O_9$ shows no spin [19] or orbital [20] freezing and may have an exotic quantum spin-orbital liquid (QSOL) ground state [17,19,21,22] which might be a consequence of disorder [18,23,24].

It is therefore important to investigate whether the same kind of disorder exists in structurally similar 6HB-$Ba_3NiSb_2O_9$ and a thorough structural study of the sample studied here has recently been undertaken [25]. Our magnetic susceptibility results are consistent with the results of Cheng *et al.* [7] yielding a Weiss constant of 75.6(6) K, a moment size of $\mu_{\rm eff} = 3.201(9)\ \mu_B$, and a similar Curie tail, thus our structural characterization should be considered to be typical of 6HB-$Ba_3NiSb_2O_9$ samples. Using x-ray, neutron, and electron diffraction, it has been shown [25] that the structure can be indexed as $P6_3/mmc$ with 50%–50% site mixing between Sb^{5+} and Ni^{2+} ions. However, at the local level, this material's structure is very different from that of $Ba_3CuSb_2O_9$ and electron diffraction measurements show that it maintains a triangular lattice of Ni ions (i.e., co-aligned Ni-Sb dumbbells) over domains roughly 10 nm in size. At the local level the structure is trigonal instead of hexagonal and the most likely explanation is that the orientation of the dumbbells alternates between adjacent planes, as shown in the inset of Fig. 1. As the magnetic exchange interactions pass primarily through Ni-O-O-Ni bonds, this structure consists of magnetic bilayers that are likely to be described by a J_1-J_2 honeycomb model. For the time being the J_1/J_2 ratio is not known.

II. MUON SPIN ROTATION

As a first step in understanding the magnetism of 6HB-$Ba_3NiSb_2O_9$, we have applied muon spin rotation (μSR), which is capable of revealing tiny fractions of a μ_B of static magnetism. The muon polarization was found to be well fit with a simple exponential decay $P(t) = \exp(-\lambda t)$, for all temperatures and longitudinal magnetic fields. Shown in Fig. 2(a) are representative polarization curves obtained in zero field (ZF). The relaxation rate $\lambda(T)$ displays a clear

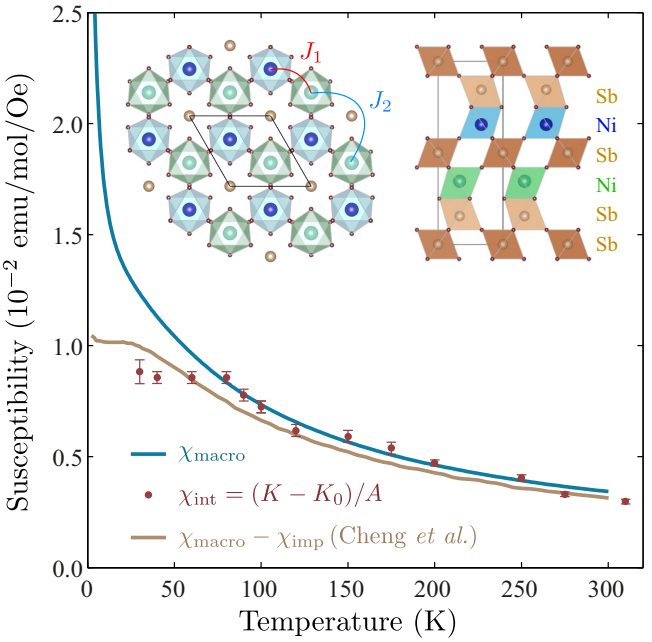

FIG. 1. The magnetic susceptibility as measured with a commercial SQUID magnetometer $\chi_{\rm macro}$ and as obtained from the NMR shift $\chi_{\rm int} = (K - K_0)/A$, with $A = -8.6$ kOe/μ_B. Also shown is the analysis of Cheng *et al.* [7] involving the subtraction of a Curie tail (scaled to match our value of $\mu_{\rm eff}$). Inset: The likely configuration of Ni^{2+} ions in the 6HB-$Ba_3NiSb_2O_9$ structure [25]. Only a select portion of the unit cell is shown to focus on the Ni ions. Given the configuration of Ni-O-O-Ni bonds, these bilayers are likely to exhibit a J_1-J_2 model on a honeycomb lattice.

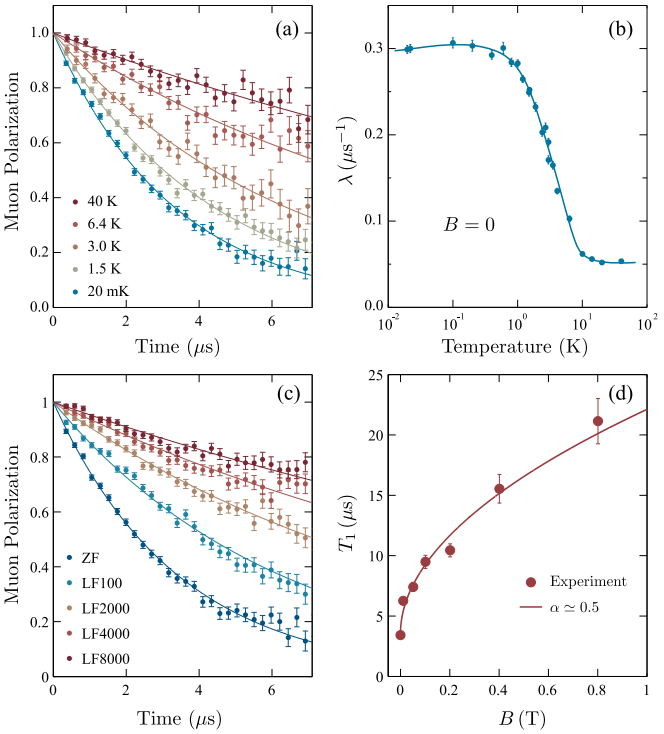

FIG. 2. (a) Representative ZF muon polarization curves $P(t)$ and exponential fits (solid lines). (b) Relaxation time $\lambda(T)$ showing a relaxation plateau below ~1 K. The solid line is a guide to the eye. (c) $P(t)$ curves for various values of longitudinal field with exponential fits. (d) Relaxation time $T_1^\mu = 1/\lambda$ as a function of longitudinal magnetic field. The solid line is a fit of the form $T_1^\mu = a + bH^\alpha$ with $\alpha = 0.52$.

plateau below ~1 K, reaching at most ~0.3 μs^{-1}. If this ZF relaxation were the result of static magnetism, it would have to be extremely weak, generating a random field distribution of width $\Gamma = \lambda/\gamma_\mu \simeq 3.5$ G. Assuming dipolar coupling to muons stopped near the oxygen atoms furthest from the Ni sites, static moments would have to be smaller than ~0.016 μ_B, a tiny fraction of the full 2.3 μ_B/Ni^{2+}. Moreover, the decoupling of this relaxation as a function of longitudinal magnetic field [Fig. 2(c)] provides definitive proof that the relaxation does not come from static moments. Such small internal fields would be quickly dwarfed by the longitudinal fields (LF) applied here, completely decoupling the muon relaxation, whereas measurable relaxation is seen in LF as high as 1 T.

The relaxation plateau of $\lambda(T)$ shown in Fig. 2(b) is by now a routine observation in a wide variety of frustrated magnetic compounds, and specifically potential QSL systems. The magnitude of the plateaus, however, can vary appreciably between systems, from $\lambda \simeq 0.05$ μs^{-1} in Herbertsmithite [2,26] and $ZnCu_3(OH)_6SO_4$ [27] to $\lambda \simeq 0.45$ μs^{-1} in Kapellasite [28] and $[NH_4][C_7H_{14}N][V_7O_6F_{18}]$ [29] to name several examples.

The decoupling curve [Fig. 2(d)] does not at all resemble the standard relation from Redfield theory [30], that is $T_1^\mu = 1/\lambda = a + bH^2$, where a and b depend on an electronic fluctuation rate ν and the fluctuating field Δ [30]. Instead we find that an unconventional power law $T_1^\mu = a + bH^\alpha$ with $\alpha = 0.52$ provides a good fit to the data. This is all the more surprising given that the relaxation is found to be exponential over the entire temperature range. Again we find a similarity to the QSL Herbertsmithite [26], where $\alpha = 0.66$, although the relaxation is overall much faster in $Ba_3NiSb_2O_9$.

III. NUCLEAR MAGNETIC RESONANCE

To offer a more local perspective on the dynamics of this material, we have employed ^{121}Sb NMR measurements. Spectra were obtained with a standard $\pi/2$-τ-π sequence with very short T_2 times requiring τ as low as 6 μs. The ^{121}Sb nuclei are strongly coupled to the magnetic Ni^{2+} spins with a hyperfine coupling of $A = -8.6$ kOe/μ_B. We cannot resolve the powder-broadened quadrupolar satellites making a proper determination of the quadrupolar coupling impossible. This is indicative of structural disorder. While there are two inequivalent Sb sites in the crystal structure, only one is seen in the NMR spectra, as is the case in $Ba_3CuSb_2O_9$ [19]. We speculate that we are able to observe the Sb nuclei that are within the Sb-Ni dumbbells and that the other Sb site, which is coupled to multiple Ni sites, is wiped out by spin fluctuations. A smaller and narrower peak with roughly zero shift is also observed. This impurity peak likely comes from a nonmagnetic parasitic phase and also exhibits a quadrupolar structure, as shown in Fig. 3(a). The impurity phase is easily distinguished from the bulk in T_2 measurements, which show two-component exponential relaxation. At low T, the T_2 of the bulk phase becomes extremely rapid (≃10 μs at 10 K),

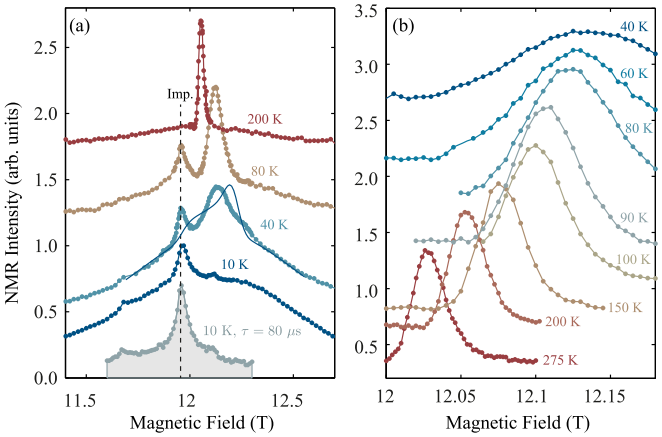

FIG. 3. (a) ^{121}Sb NMR spectra at selected temperatures showing the main line and impurity peak. One spectrum (gray) with $\tau = 80\ \mu$s reveals only the slowly relaxing impurity contribution. The strong anisotropy predicted by Serbyn *et al.* [12] is inconsistent with the data, as shown by the powder simulation over the 40 K data (thin blue curve). (b) The majority signal shows an appreciable shift $K(T)$.

whereas T_2 of the impurity phase becomes longer, as shown in Fig. 4. Although it represents only about 2% of the sample, the impurity phase contributes heavily to the spectra because of its longer T_2.

The temperature dependence of the NMR shift $K(T)$ yields the intrinsic susceptibility shown in Fig. 1. It increases with decreasing temperature until reaching a plateau near 60 K. Below 30 K or so, it becomes impossible to resolve the shift precisely due to the influence of the impurity site, but the spectral weight does remain appreciably shifted down to the lowest temperatures studied. This confirms the hypothesis of Cheng *et al.* [7] that an orphan spin contribution (of the order

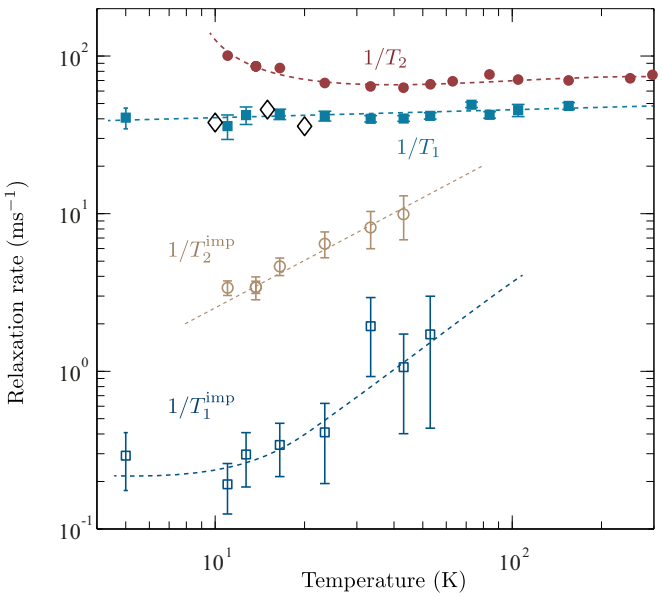

FIG. 4. ^{121}Sb NMR relaxation rates: $1/T_1$ of the bulk (■) and of the impurity site (□), and $1/T_2$ of the bulk (●) and impurity site (○). The black diamonds (◊) are $1/T_1$ obtained with a contrast measurement. Dashed lines are guides to the eye.

of 1.7%) must be subtracted from $\chi_{\rm macro}$ to obtain the true, intrinsic susceptibility $\chi_{\rm int}$ which we prove to remain finite and largely constant at low temperature. A significantly larger Curie tail (representing roughly 15% of Cu spins) is found in $Ba_3CuSb_2O_9$ [19] which has a natural explanation in its very short-range ordered structure [18].

In the spin-lattice relaxation (T_1) recovery curves, two components are also observed. With two-component fits (see the Appendix), we extract the values of $1/T_1$ for the majority phase and nonmagnetic impurity (squares in Fig. 4). To more rigorously confirm that this simple analysis accurately determines the T_1 of the majority phase, we have used a contrast method (described in detail in the Appendix) to remove most of the impurity signal. The resulting fits give the black diamonds in Fig. 4 and confirm our two-component analysis. The resulting value of $1/T_1$ is essentially independent of temperature, varying at most as $T^{0.1}$. A constant spin-lattice relaxation rate is relatively rare, though in several spin chain systems it varies very little or has only a slight logarithmic increase at low temperatures [31,32]. Similar physics could be at play here. While clearly these results extend well below Θ_W, we could consider the possibility that frustration lowers the onset of spin correlations, placing our NMR measurements in a paramagnetic regime, which would also lead to a constant T_1. Following Ref. [33], with parameters relevant to 6HB-$Ba_3NiSb_2O_9$, we obtain $1/T_1 \simeq 7.45\ \text{ms}^{-1}$ in the paramagnetic limit, which is not so distant from the measured values of 40–50 ms^{-1}.

The NMR experiments become difficult as the temperature is lowered due to a shrinking T_2, thus our NMR results do not overlap appreciably with the μSR plateau. However, the NMR data at 5 K are somewhat inconsistent with the onset of the relaxation plateau. μSR has the advantage of extending to much lower temperatures without loss of signal, but since it is a less local probe the plateau may arise from coupling to dilute impurities (orphan spins), to which NMR is less sensitive. This has been proposed as a possible explanation for the relaxation plateau in Herbertsmithite [26], where the NMR $1/T_1$ is an increasing function of temperature [34]. A similar contrast between μSR and NMR was more recently seen in the kagome system $ZnCu_3(OH)_6SO_4$ [27] and in the triangular organic QSL κ-(BEDT-TTF)$_2$Cu$_2$(CN)$_3$ [35,36].

The spin-lattice relaxation rate can be determined with $1/T_1 = (\gamma^2 k_B T/\omega_0)\sum_q |A(q)|^2 \chi''_\perp(q,\omega_0)$, so to directly compare NMR and μSR we must look above the relaxation plateau, at the same Larmor frequency (the ^{121}Sb nucleus at 12 T has roughly the same Larmor frequency as muons at ~0.9 T), and scale the relaxation rates by $\gamma^2 A^2$, assuming that there is no significant q dependence. As before, we take a muon stopping site roughly 4 Å away from the Ni ions and assume that the decoupling curve illustrated in Fig. 2(d) holds everywhere. Under these assumptions, we expect an NMR $1/T_1$ to be roughly 58 ms^{-1}, in rather good agreement with the measured relaxation rate.

IV. DISCUSSION

Having confirmed that 6HB-$Ba_3NiSb_2O_9$ shows no static magnetism down to 20 mK and appears to have gapless spin excitations, we now consider possible reasons for such

exotic physics. These results are indeed puzzling given that a spin-1/2 triangular-lattice antiferromagnet is expected to order in the 120° structure. Similarly, the standard honeycomb lattice is bipartite and would support a simple antiferromagnetic order. Evidently additional frustrating parameters must be considered.

We first consider a scenario wherein the exchange interaction is modulated by disorder, giving rise to a random exchange model on the triangular lattice. In recent theoretical work (see Refs. [37,38]), exchange randomness, above a critical value of $\Delta J_C/J = 0.5 \pm 0.15$, in a $S = 1/2$ triangular lattice model was shown to induce a random singlet QSL-like state with gapless spin excitations and a linear specific heat. However, a significant level of disorder in the exchange interaction would lead to a proportional disorder in the local susceptibility which is one of several possible sources of NMR line broadening. The measured linewidths place a conservative upper limit on the exchange disorder of $\Delta J/J \lesssim 0.25$. It is also worth noting that $\Delta\chi/\chi$ is much smaller here than in $Ba_3CuSb_2O_9$ (roughly 7 times as large at 80 K for example) [19], supporting the conclusion [25] that 6HB-$Ba_3NiSb_2O_9$ is much less disordered at the local level. We therefore conclude that structural disorder cannot explain the observed gapless QSL-like physics.

Supposing that the in-plane exchange, J_2, is the dominant interaction strength, this system may be adequately described by triangular lattice models. Several different varieties of QSL have been proposed for $S = 1$ triangular antiferromagnets based on models that incorporate biquadratic exchange, next-nearest-neighbor exchange, interlayer exchange, and/or single ion anisotropy [11–14,16]. One of these theories has provided experimental predictions that can be tested with the present experiments [12,13]. Specifically, Serbyn *et al.* [12] have considered biquadratic exchange and single-ion anisotropy and have proposed a chiral QSL that reproduces the linear $C(T)$, constant $\chi(T)$, and Wilson ratio R_W. They predict an exponentially vanishing $1/T_1$ but this is clearly at odds with our observation of a constant $1/T_1$ in NMR and relaxation plateau in μSR (although the NMR results do not rule out a small gap $\lesssim$2 K or so). Second, they predict a strong anisotropy $\chi_{xx} = \chi_0$ and $\chi_{zz} = 0$ at low T. The macroscopic (SQUID) susceptibility measurement of a powder is simply a weighted sum of these terms giving $\chi_{\text{powder}} = 2\chi_{xx}/3 + \chi_{zz}/3$, and thus is not in conflict with this prediction. However, NMR provides a *histogram* of susceptibilities and in the case of strong anisotropy would give an intense peak at $B(1 - A\chi_{xx}) = 12.19$ T along with a hump at $B(1 - A\chi_{zz}) = 11.96$ T. This peak-hump structure is not consistent with our data, as shown by the solid line in Fig. 3(a).

Chen *et al.* [15], meanwhile, do away with QSL physics and instead consider the possibility that this system is near to a quantum critical point (QCP) driven by anisotropy D. Depending on the precise value of D either a gap and strong anisotropy or else a small ordered moment can be expected. Again, both of these scenarios are ruled out, provided the gap is not especially small. Several other QSL theories have been proposed that may still apply to this system, but that have not made predictions that can be tested with our experiments [11,14,16].

If J_2 and J_1 are comparable in strength, a frustrated honeycomb model may be more relevant to this system. Two sources of frustration for $S = 1$ spins on the honeycomb lattice have been considered from a theoretical point of view: competition between bilinear and biquadratic interactions [39] or a J_1-J_2 Heisenberg model [40]. In both cases, a range of parameters leads to a plaquette valence bond crystal (VBC) ground state. Such a state is also found in the frustrated $S = 1/2$ case [41–43]. A VBC ought to have gapped spin excitations and thus does not appear to be consistent with our results. Thus, it may be that the present system exists at a deconfined QCP between plaquette VBC and antiferromagnetic order which is seen in at least two of the aforementioned models [39,42].

In conclusion, our μSR and NMR results show that 6HB-$Ba_3NiSb_2O_9$ is a good gapless QSL candidate with no static magnetism, constant χ, constant T_1 in NMR, and a μSR relaxation plateau at low temperatures. Despite the inherent disorder in this system, our NMR linewidths indicate that disorder alone is not sufficient to induce a QSL ground state as considered in Ref. [37]. We can likely rule out two particular theoretical models [12,15], leaving several theories of QSL [11,14] or of deconfined quantum criticality [39,40,42] that may be applicable to this system. Theoretical predictions for the NMR line shape and relaxation rates in these models are therefore an important future research direction.

ACKNOWLEDGMENTS

Thanks to P. Bordet, C. Lepoittevin, H. Klein, S. Kodjikian, and C. Colin for assistance with sample characterization. We acknowledge helpful discussions with S. Bieri, C. Lhuillier, B. Fåk, C. Bourbonnais, F. Mila, S. Gong, and L. Balents. This work was supported by the French Agence Nationale de la Recherche under Grant "SPINLIQ" No. ANR-12-BS04-0021, Université Paris-Sud Grant MRM PMP and the Triangle de la physique, Contract No. 084004, as well as the National Sciences and Engineering Research Council (NSERC) of Canada.

APPENDIX A: SEPARATION OF INTRINSIC AND IMPURITY SIGNALS

The NMR signal was obtained with a standard Hahn spin-echo sequence $\pi/2$-τ-π. Spectra were obtained by integrating the spin echo intensity at constant frequency while the magnetic field was varied. The spin-spin relaxation time T_2 was obtained by varying τ in the aforementioned sequence. Varying τ has also allowed us to highlight slowly or quickly relaxing components of the signal. In the limit $\tau \to 0$ we should observe the correct relative intensities of the different components in the sample. As τ becomes larger, the weight of slowly relaxing components becomes more significant.

The sample of 6HB-$Ba_3NiSb_2O_9$ that we have studied shows two primary components in the NMR spectra. The majority phase is found to be very fast relaxing (T_2 is as short as 10 μs depending on the temperature). A minority phase is also observed that has very little line shift and is much more slowly relaxing. This phase is therefore very likely a

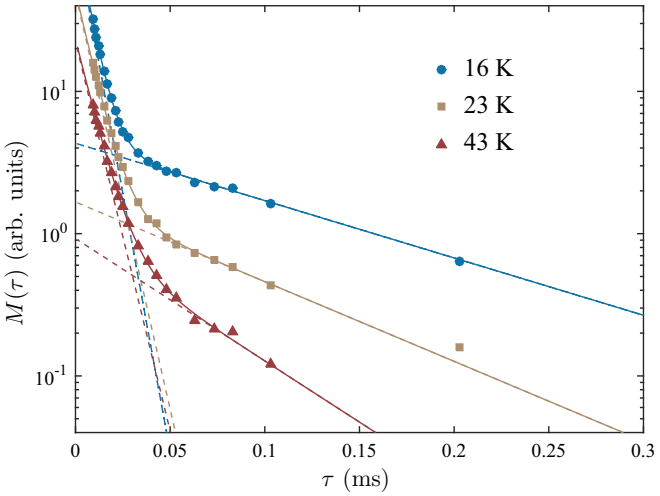

FIG. 5. Spin-spin relaxation curves $M(\tau)$ at several temperatures, showing clear two-component exponential relaxation. The solid lines are double exponential fits. The dashed lines are extrapolations of the individual exponential components which appear as straight lines on a semilog plot.

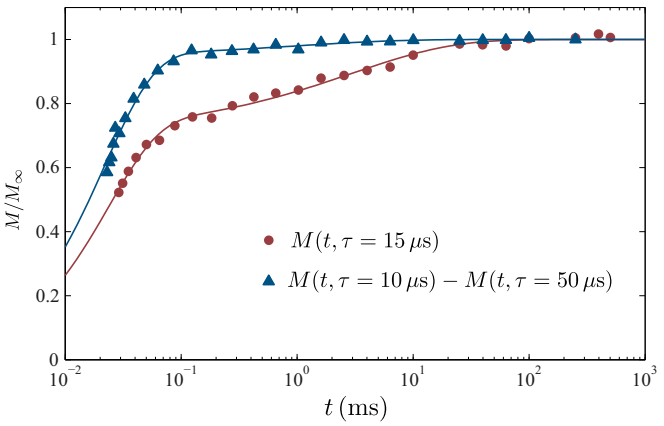

FIG. 6. Spin-lattice relaxation recovery curves obtained at 10 K with a standard method (red) and with a contrast method that almost completely eliminates slowly relaxing components (blue). The fits are described in the text.

nonmagnetic impurity phase. In Fig. 3(a) spectra are shown at various temperatures taken with $\tau < 10$ μs. One spectrum acquired with $\tau = 80$ μs at 10 K is also shown (gray curve). In this spectrum, the majority phase is all but eliminated and what remains is the nonmagnetic impurity signal. We see that this phase also has a quadrupolar splitting that leads to a narrow peak superimposed on a broad powder-broadened quadrupolar contribution. We do resolve two of the quadrupolar satellite peaks of this component. For relaxation measurements, we worked at a part of the spectrum away from the narrow central peak of the impurity component but the fact that this contribution also has a broad quadrupolar component means that we cannot completely avoid it. Special care was therefore taken to isolate the main-phase and nonmagnetic impurity components in relaxation measurements.

Shown in Fig. 5 are $M(\tau)$ spin-spin relaxation curves at several different temperatures and at fields away from the impurity peak. Clear two-component exponential relaxation (straight lines in the semilog plot) is seen, consistent with our interpretation of the spectra. While the intrinsic component dominates in a time window from 0 to $\sim$30 μs, that of the impurity phase is isolated at long times. These two-component fits have been used to generate the $1/T_2(T)$ results shown in Fig. 4. Whereas the main phase T_2 gets shorter as the temperature is reduced, the nonmagnetic impurity phase gets much longer. This enabled us to perform "contrast" experiments where at long times we obtain only the nonmagnetic impurity contribution, while at short times the intrinsic contribution represents the dominant component of the spectrum. Given the broadening of the latter, especially at low temperature, the very small impurity phase appears to have a large contribution to the spectra at the unshifted position, since it is impossible to work at $\tau = 0$. Extrapolating to $\tau = 0$ allows us to estimate that the nonmagnetic impurity phase represents roughly 2% of the Sb sites in the sample.

The spin-lattice relaxation rate was measured using the saturation-recovery method, that is applying the sequence $\pi/2$-t-$\pi/2$-τ-π and determining $M(t)$. However, due to very fast relaxation, we were unable to reach the point of full saturation. To carefully define our $\pi/2$ saturation pulse, we performed tests on a different Sb-containing compound in the same probe and coil. Once again, we see evidence of two components in the recovery curves, as can be seen in Fig. 6. Two methods to extract the intrinsic T_1 have been used which give consistent results.

The first method relies on the aforementioned contrast technique. Since the nonmagnetic impurity phase is slowly relaxing, changing τ from 10 to 50 μs barely alters its amplitude. However, at $\tau = 50$ μs, the main phase has been reduced by an order of magnitude or more (see Fig. 5). Thus obtaining recovery curves for these two different values of τ and subtracting them allows us to almost completely eliminate the nonmagnetic impurity phase while hardly altering the majority phase. These two measurements were performed simultaneously, under identical experimental conditions, before being subtracted. The result is shown as the blue curve in Fig. 6. Evidently the slowly relaxing component is eliminated and only a fast exponential remains. Performing exponential fits to recovery curves obtained in this way, we generate the black diamonds in Fig. 4.

A simpler analysis scheme is to use a two-component fit to analyze the recovery curves. Because of disorder or quadrupolar channels to relaxation, the nonmagnetic impurity phase was best fit with a stretched exponential (with $\beta \simeq 0.5$). Thus the data were fit with the following equation:

$$M(t) = M_\infty\left[1 - ae^{-t/T_1} - a_{\rm imp}e^{-(t/T_1^{\rm imp})^\beta}\right].$$

This two-component fit method, shown as the red curve in Fig. 6, was used to generate the $1/T_1(T)$ data points shown as the open and closed blue squares in Fig. 4. These data points match well with the results of the contrast method, thus validating our interpretation of the data.

[1] L. Balents, Nature **464**, 200 (2010).

[2] P. Mendels, F. Bert, M. A. de Vries, A. Olariu, A. Harrison, F. Duc, J. C. Trombe, J. Lord, A. Amato, and C. Baines, Phys. Rev. Lett. **98**, 077204 (2007).

[3] T.-H. Han, J. S. Helton, S. Chu, D. G. Nocera, J. A. Rodriguez-Rivera, C. Broholm, and Y. S. Lee, Nature (London) **492**, 406 (2012).

[4] Y. Shimizu, K. Miyagawa, K. Kanoda, M. Maesato, and G. Saito, Phys. Rev. Lett. **91**, 107001 (2003).

[5] S. Yamashita, Y. Nakazawa, M. Oguni, Y. Oshima, H. Nojiri, Y. Shimizu, K. Miyagawa, and K. Kanoda, Nat. Phys. **4**, 459 (2008).

[6] I. Affleck, J. Phys.: Condens. Matter **1**, 3047 (1989).

[7] J. G. Cheng, G. Li, L. Balicas, J. S. Zhou, J. B. Goodenough, C. Xu, and H. D. Zhou, Phys. Rev. Lett. **107**, 197204 (2011).

[8] Y. Shirata, H. Tanaka, T. Ono, A. Matsuo, K. Kindo, and H. Nakano, J. Phys. Soc. Jpn. **51**, 2424 (1982).

[9] J. Hwang, E. S. Choi, F. Ye, C. R. Dela Cruz, Y. Xin, H. D. Zhou, and P. Schlottmann, Phys. Rev. Lett. **109**, 257205 (2012).

[10] P. D. Battle, C. W. Jones, P. Lightfoot, and R. Strange, J. Solid State Chem. **85**, 144 (1990).

[11] C. Xu, F. Wang, Y. Qi, L. Balents, and M. P. A. Fisher, Phys. Rev. Lett. **108**, 087204 (2012).

[12] M. Serbyn, T. Senthil, and P. A. Lee, Phys. Rev. B **84**, 180403(R) (2011).

[13] S. Bieri, M. Serbyn, T. Senthil, and P. A. Lee, Phys. Rev. B **86**, 224409 (2012).

[14] K. Hwang, T. Dodds, S. Bhattacharjee, and Y. B. Kim, Phys. Rev. B **87**, 235103 (2013).

[15] G. Chen, M. Hermele, and L. Radzihovsky, Phys. Rev. Lett. **109**, 016402 (2012).

[16] M. Moreno-Cardoner, H. Perrin, S. Paganelli, G. De Chiara, and A. Sanpera, Phys. Rev. B **90**, 144409 (2014).

[17] S. Nakatsuji, K. Kuga, K. Kimura, R. Satake, N. Katayama, E. Nishibori, H. Sawa, R. Ishii, M. Hagiwara, T. U. Ito *et al.*, Science **336**, 559 (2012).

[18] A. Smerald and F. Mila, Phys. Rev. Lett. **115**, 147202 (2015).

[19] J. A. Quilliam, F. Bert, E. Kermarrec, C. Payen, C. Guillot-Deudon, P. Bonville, C. Baines, H. Luetkens, and P. Mendels, Phys. Rev. Lett. **109**, 117203 (2012).

[20] Y. Ishiguro, K. Kimura, S. Nakatsuji, S. Tsutsui, A. Q. R. Baron, T. Kimura, and Y. Wakabayashi, Nat. Commun. **4**, 1 (2013).

[21] H. D. Zhou, E. S. Choi, G. Li, L. Balicas, C. R. Wiebe, Y. Qiu, J. R. D. Copley, and J. S. Gardner, Phys. Rev. Lett. **106**, 147204 (2011).

[22] N. Katayama, K. Kimura, Y. Han, J. Nasu, N. Drichko, Y. Nakanishi, M. Halim, Y. Ishiguro, R. Satake, E. Nishibori *et al.*, Proc. Natl. Acad. Sci. USA **112**, 9305 (2015).

[23] A. Smerald and F. Mila, Phys. Rev. B **90**, 094422 (2014).

[24] P. Corboz, M. Lajko, A. M. Lauchli, K. Penc, and F. Mila, Phys. Rev. X **2**, 041013 (2012).

[25] C. Darie, C. Lepoittevin, H. Klein, S. Kodjikian, P. Bordet, C. V. Colin, O. I. Lebedev, C. Deudon, and C. Payen, J. Solid State Chem. **237**, 166 (2016).

[26] E. Kermarrec, P. Mendels, F. Bert, R. H. Colman, A. S. Wills, P. Strobel, P. Bonville, A. Hillier, and A. Amato, Phys. Rev. B **84**, 100401(R) (2011).

[27] M. Gomilšek, M. Klanjšek, M. Pregelj, F. C. Coomer, H. Luetkens, O. Zaharko, T. Fennell, Y. Li, Q. M. Zhang, and A. Zorko, Phys. Rev. B **93**, 060405 (2016).

[28] B. Fak, E. Kermarrec, L. Messio, B. Bernu, C. Lhuillier, F. Bert, P. Mendels, B. Koteswararao, F. Bouquet, J. Ollivier *et al.*, Phys. Rev. Lett. **109**, 037208 (2012).

[29] L. Clark, J. C. Orain, F. Bert, M. A. de Vries, F. H. Aidoudi, R. E. Morris, P. Lightfoot, J. S. Lord, M. T. F. Telling, P. Bonville *et al.*, Phys. Rev. Lett. **110**, 207208 (2013).

[30] C. P. Slichter, *Principles of Magnetic Resonance, Third Enlarged and Updated Edition* (Springer, Berlin, 1989).

[31] R. Nath, A. V. Mahajan, N. Büttgen, C. Kegler, A. Loidl, and J. Bobroff, Phys. Rev. B **71**, 174436 (2005).

[32] V. Barzykin, Phys. Rev. B **63**, 140412 (2001).

[33] T. Moriya, Prog. Theor. Phys. **16**, 23 (1956).

[34] M. Jeong, F. Bert, P. Mendels, F. Duc, J. C. Trombe, M. A. de Vries, and A. Harrison, Phys. Rev. Lett. **107**, 237201 (2011).

[35] S. Nakajima, T. Suzuki, Y. Ishi, K. Ohishi, I. Watanabe, T. Goto, A. Oosawa, N. Yoneyama, N. Kobayashi, F. L. Pratt, and T. Sasaki, J. Phys. Soc. Jpn. **81**, 063706 (2012).

[36] T. Itou, A. Oyamada, S. Maegawa, and R. Kato, Nat. Phys. **6**, 673 (2010).

[37] K. Watanabe, H. Kawamura, H. Nakano, and T. Sakai, J. Phys. Soc. Jpn. **83**, 034714 (2014).

[38] T. Shimokawa, K. Watanabe, and H. Kawamura, Phys. Rev. B **92**, 134407 (2015).

[39] H. H. Zhao, C. Xu, Q. N. Chen, Z. C. Wei, M. P. Qin, G. M. Zhang, and T. Xiang, Phys. Rev. B **85**, 134416 (2012).

[40] S.-S. Gong, W. Zhu, and D. N. Sheng, Phys. Rev. B **92**, 195110 (2015).

[41] D. C. Cabra, C. A. Lamas, and H. D. Rosales, Phys. Rev. B **83**, 094506 (2011).

[42] D. J. J. Farnell, R. F. Bishop, P. H. Y. Li, J. Richter, and C. E. Campbell, Phys. Rev. B **84**, 012403 (2011).

[43] A. F. Albuquerque, D. Schwandt, B. Hetényi, S. Capponi, M. Mambrini, and A. M. Lauchli, Phys. Rev. B **84**, 024406 (2011).